LA-UR-20-24387 (Accepted Manuscript)

A Short-lived Three-Belt Structure for sub-MeV Electrons in the Van Allen Belts: Time Scale and Energy Dependence

Hao, Y. X.; Zong, Qiugang; Zhou, X. Z.; Zou, H.; Rankin, R.; Sun, Y. X.; Chen, X. R.; Liu, Y.; Fu, S. Y.; Baker, D. N.; Spence, H. E.; Blake, J. B.; Reeves, Geoffrey D.; Claudepierre, S. G.

To be published in: Journal of Geophysical Research: Space Physics

DOI to publisher's version: 10.1029/2020JA028031

Permalink to record: http://permalink.lanl.gov/object/view?what=info:lanl-repo/lareport/LA-UR-20-24387

A Short-lived Three-Belt Structure for Sub-MeV Electrons in the Van Allen Belts: Time Scale and Energy Dependence

Y. X. Hao[1], Q. -G. Zong[1], X. -Z. Zhou[1], H. Zou[1], R. Rankin[2], Y. X. Sun[1], X. R. Chen[1], Y. Liu[1], S. Y. Fu[1], D. N. Baker[3], H. E. Spence[4], J. B. Blake[5], G. D. Reeves[6] and S. G. Claudepierre[5,7]

Q.-G. Zong, Institute of Space Physics and Applied Technology, Peking University.(qgzong@pku.edu.cn)

[1]Institute of Space Physics and Applied Technology, Peking University, Beijing, China.

[2]Department of Physics, University of Alberta, Edmonton, Alberta,Canada.

[3]Laboratory for Atmospheric and Space Physics, University of Colorado, Boulder, Colorado, USA.

[4]Department of Physics Institute for Earth, Oceans and Space, University of New Hampshire, Durham, New Hampshire, USA.

Abstract.

In this study we focus on the radiation belt dynamics driven by the geomagnetic storms during September 2017. Besides the long lasting three-belt structures of ultra-relativistic electrons (>2 MeV, existing for tens of days), which has been studied intensively during the Van Allen Probe era, it is found that magnetospheric electrons of hundreds of keVs can also have three-belt structures at similar L extent during storm time. Measurements of 500 keV∼ 800 keV electrons from MagEIS instrument onboard Van Allen Probes show double-peaked ($L = 3.5$ and 4.5 respectively) flux-versus-L-shell profile in the outer belt, which lasted for 2-3 days. During the time interval of such transient three-belt structure, the energy-versus-L spectrogram show novel distributions differing from both“S-shaped” and “V-shaped” spectrograms

[5]Space Science Applications Laboratory, The Aerospace Corporation, El Segundo, California, USA

[6]Los Alamos National Laboratory, Los Alamos NM USA and The New Mexico Consortium, Los Alamos NM, USA.

[7]Department of Atmospheric and Oceanic Sciences, University of California, Los Angeles, CA, USA.

reported previously. Such peculiar distribution also illustrates the energy dependent occurrence of the three-belt profile. The gradual formation of "reversed energy spectrum" at $L \sim 3.5$ also indicates that hiss scattering inside the plasmapause contributed to the fast decay of sub-MeV remnant belt.

1. Introduction

Since their discovery in late 1950s [*Van Allen et al.*, 1958; *Van Allen*, 1959; *Van Allen and Frank*, 1959], the morphology and evolution of the radiation belts surrounding Earth have been a fundamental topic of space physics. Multiple processes dominating the acceleration, loss and transport of relativistic ($>\sim$500 keV) and ultra-relativistic ($>\sim$2 MeV) [e.g., *Mann et al.*, 2016] have been discussed and their competing contributions to radiation belt dynamics have been hotly debated. Energetic particle measurement with unprecedented resolution in energy, space and time from Van Allen Probes mission revealed plenty of unexpected features of the electron radiation belts.

One of the most textbook-rewriting discovery during the Van Allen Probes era is the three-belt structure of ultra-relativistic electrons [*Baker et al.*, 2013b]. A previously unseen "storage ring" of intense ultra-relativistic electron flux stood out between the slot region and the outer belt after 2 September 2012 and lasted for weeks. Such ultra-relativistic three-belt structure were also found in SAMPEX data sets. Eight SAMPEX three-belt events of 1.5-6.0 MeV electrons during both CME- and CIR-driven storms were reported by *Yuan and Zong* [2013]. Focusing on the energy range from 1.8 MeV to 7.6 MeV, statistical study by *Pinto et al.* [2018] reported 30 three-belt events during the first five years of Van Allen Probes mission. *Mann et al.* [2013] suggested that such three-belt structure can be formed by radial transport of electrons driven by ultra-low-frequency waves. In most of the ultra-relativistic three-belt events, the storage ring (otherwise termed as "remnant belt") that had survived from the outer belt dropout lasted for more than 10 days. Such an unusual persistence of the ultra-relativistic storage ring has been attributed to the low efficiency of hiss wave scattering in that energy range [*Shprits et al.*, 2013].

Unlike the ultra-relativistic electrons, electrons with energy $<$1 MeV have been found to be quite sensitive to scattering caused by hiss waves. After the filling process of the outer belt, which commonly leaves a "V-shaped" distribution in energy versus L spectrogram [*Reeves et al.*, 2016], hiss waves inside the plasmasphere could deplete the flux of sub-MeV electrons by scattering them to atmosphere, causing an "S-shaped" distribution [*Ripoll et al.*, 2016]. The slice of an S-shaped distribution at certain L shell yields bump-on-tail spectrum, which has been found to dominate inside the plasmasphere [*Zhao et al.*, 2019b]. *Zhao et al.* [2019a] also suggested that the bump-on-tail spectra with a valley at sub-MeV energy range are formed by energy-preferential loss through hiss wave scattering.

To date, all the three-belt events reported are in the energy range $>$1 MeV, due to the attention on ECT-REPT (on Van Allen Probes) [e.g., *Baker et al.*, 2013b; *Mann et al.*, 2013; *Pinto et al.*, 2018] and PET (on SAMPEX) [e.g., *Yuan and Zong*, 2013] data sets. Three-belt structure has not been regarded as a type of morphology for sub-MeV electrons. However, all the processes that are essential to form a three-belt structure, namely, partial dropout and subsequent replenishment in favorable radial extent, are sure to happen in both ultra-relativistic and sub-MeV energy range. In this work, we report a three-belt event in the energy range 529 keV$\sim$814 keV that lasted only for $\sim$2 days. Its time evolution, unenduring nature and energy dependence are investigated and compared with the well-documented ultra-relativistic three-belt structures. Based on electron spectral evolutions during this event, we demonstrate that the formation of a sub-MeV three-belt structure can be driven by the similar mechanism as previously discussed ultra-relativistic three-belt but its remnant belt may decay faster due to more efficient pitch angle scattering and henceforth faster precipitation to atmosphere driven by hiss waves. Besides, novel types of electron distributions in energy spectrogram and phase space density profile are revealed, adding to broader knowledge on the morphology of terrestrial radiation belt.

2. Instrumentation

In this work we focus on measurements from Magnetic Electron Ion Spectrometer (MagEIS) [*Blake et al.*, 2013] of Energetic Praticle, Composition, and Thermal plasma (ECT) suite [*Spence et al.*, 2013] onboard Van Allen Probe A and B [*Mauk et al.*, 2014] to reveal the three-belt structure of hundreds of keVs during September 2017. Background-corrected fluxes [*Claudepierre et al.*, 2015] are used to avoid contaminations due to protons and bremsstrahlung X-rays. Relativistic Electron Proton Telescope (REPT) [*Baker et al.*, 2013a] measurements provide the ≥1.8 MeV part of the electron energy spectra. BeiDa Image Electron Spectrometer (BD-IES)[*Zong et al.*, 2016, 2018; *Zou et al.*, 2018] onboard a Chinese 55° inclined geosynchronous orbit satellite provides the fluxes of 50 $\sim$ 600 keV electrons above $L = 6.6$, which serve as the outward boundary condition of the outer radiation belt in this study.

Magnetic field strength from Electric and Magnetic Field Instrument Suite and Integrated Science (EMFISIS) [*Kletzing et al.*, 2012] is used when calculating electron phase space density (PSD) from MagEIS flux data. Geomagnetic indices and solar wind parameters shifted to terrestrial magnetopause presented in this article are provided by NASA OMNI database (http://omniweb.gsfc.nasa.gov/).

3. Transient Three-belt Event of Sub-MeV Electrons in September 2017

3.1. Precondition of the Three-belt Event

Figure 1 presents the geomagnetic indices and evolution of terrestrial radiation belts from 1 to 24 September 2017. Two halo coronal mass ejections (CME) related with M2.4 and X9.3 X-ray flares in AR12673 region were launched from the sun at 2028UT on 4 September and 1153UT on 6 September. The interplanetary shocks ahead of these two CMEs impinged terrestrial magnetosphere separately at 2345UT on 6 September and 2300UT one day later, leading to increases of +40 and +50nT in SYM/H index and magnetopause's being compressed into $L < 8$ region. Dropout of the outer belt electrons was recorded by both Van Allen Probes and BD-IES at the heart and the outward boundary of the outer belt immediately after the passage of the high pressure solar wind (fluxes of 500∼600 keV channel presented in Figure 1), which can be explained as the shadowing effect of the sudden compressed magnetopause to the particles' drift orbit and possible outward diffusion that follows [e.g., *Turner et al.*, 2012].

Consecutive passage of two CME structures triggered an intense geomagnetic storm with double dips in Dst (also SYM/H) index, which is similar to the time profile of the well-known March 2003 storm [e.g., *Farrugia et al.*, 2006]. On 8 September, dips of -145nT and -120nT emerged on 0100UT and 1800UT in SYM/H index (Dst = -124nT and -109nT correspondingly). The outer belt was replenished rapidly right after the first dip of the storm and the acceleration process continued during the recovery phase of the storm, (from 9 to 12 September). As shown in Figure 1, flux enhancement in 500 ∼ 600 keV channel was observed both at the heart and outer boundary of the outer belt by MagEIS and BD-IES. Note that the flux enhancement happened throughout MagEIS channels, please check Figure S1 for other channels. As to the ∼600 keV channel, electrons gradually penetrated into L = 2.5 region from 8 September to 10 September and stayed there for several days, which gave rise to the precondition of the subsequent third belt event to be discussed in this article.

3.2. Three-belt Structure After a Dynamic Pressure Pulse

A solar wind dynamic pressure pulse accompanied by fluctuating IMF B_z impinged magnetosphere at 2005UT on 12 September, right after the recovery phase of the previous intense storm. The arrival of the pressure pulse was recorded by an increase of +29 nT in SYM/H time profile, and was followed by a moderate storm (minimum SYM/H = -70 nT at 0012UT on 13 September). As shown in Figure 1, magnetopause stand-off distance (calculated according to *Shue et al.* [1998]) dropped to L = 7 region due to the pressure pulse. Flux depletion of 500∼600 keV electron at $L > 4$ was recorded by BD-IES and MagEIS after the pressure pulse impingement, while the electrons inside L = 4 seems to remain unaffected by the pressure pulse. During the recovery phase of the moderate storm, the $L > 4$ region was refilled, leaving a slot-like local flux minimum at $L \sim 4$. Such process forms a three-belt structure, which lasted for about 2 days in ∼600 keV channel in this event. Such a three-belt structure was most significant in the 529-667 keV channel (centered at 599.6 keV, therefore henceforth referred to as 600 keV three-belt structure) in MagEIS-B and was also slightly recognizable in 667.2-813.7keV (centered at 742.5keV), not appeared in other energy channels during the time interval. Please check Figure 5(c) and Figure S1 for more details.

Figure 2 presents a zoom-in view of the time interval 12 September - 15 September (marked with the small green color box in Figure 1). As marked by the black dashed line in panel (f), the pre-existing outer belt (henceforth referred to as "remnant belt") peaked at L = 3.5 and was gradually decaying during the time interval. A newly-born belt (henceforth referred to as "external outer belt") emerged above L = 4 on 13 September and peaked at $L \sim 4.5$. On 15 September, the remnant belt was no longer recognizable in the 600 keV channel. The radiation belt turned back to double-belt structure again, while the "outer belt" has already been replaced by the new populations accelerated during the recovery phase of the 13 Sep storm.

Panel (a) - (e) of Figure 2 present the energy-dependent evolution of the radiation belt in the format of $j(E_k, L)$ snapshots (same format as *Reeves et al.* [2016]). As shown in panel (a), before the pressure pulse arrival, the radiation belt show typically "V-shaped" boundaries at slot region in energy-versus-L-shell plane, which is frequently observed by Van Allen Probes after the outer belt enhancement events [cf. *Reeves et al.*, 2016, Figure 11]. As marked with the black arrow, the flux maximum of outer belt appeared at L = 3.5, which corresponds to the remnant belt populations (black arrows have been plotted at the same place in the rest panels). The energy-spatial distribution of electrons shown in panel (a) could be regarded as the initial condition of the three-belt event discussed in this work, which was largely formed by the recovery phase of the intense storm discussed in the Section 3.1.

Comparing the $j(E_k, L)$ snapshots plotted in Figure 2 (a) - (e) in a chronological sequence, one can tell that there are two predominant processes driving the developing and fading-out of the three-belt structures: the decaying of the remnant belt and the emerging of the external belt. As shown in panel (b), the flux maximum of >500 keV electrons at L = 3.5 persisted after the pressure pulse passage while the flux of <500 keV electrons began to intensify at $L > 4$. The flux enhancement at $L > 4$ extended to higher energy channels in panel (c), leading to a tri-peak distribution in $j(E_k, L)$. The fading of the remnant belt and the flux enhancement of the external belt continued in panel (d) and (e). Finally, the local flux maximum at L =3.5 was no longer observed and the $j(E_k, L)$ snapshot turned back to "V-shaped", while the outer boundary of "V" has been replaced by the new external outer belt accelerated during the moderate magnetic storm.

We note that during the period of three-belt event of 600 keV channel (see Figure 2 (c) and (d)), the flux of radiation belt electrons as a function of energy and L shell presented peculiar distributions significantly different from the well-known "S-shaped" or "V-shaped" contours [*Reeves et al.*, 2016; *Ripoll et al.*, 2016; *Turner et al.*, 2019]. At $L < 4$, the outer belt population accelerated by the previous intense storm was not completely depleted after the pressure pulse arrival. Meanwhile at $L = 4 \sim 5$, the new populations were gradually emerging and penetrated to deeper L shell at lower energy channels. One may term such kind of $j(E_k, L)$ distributions as "V-shaped distributions with a remnant belt". Another noteworthy observational feature is that, in Figure 2 (d), the outer boundary of the slot region was "S-shaped" (as pointed by the red arrow), which indicates an energy preferential decaying process at $L = 3.1 \sim 3.5$. The energy-dependent decaying process of the remnant belt will be discussed in detail in Section 5.

4. Temporal Evolution of Two Outer Belts in Phase Space Density Profile

In the previous section, the evolutions of the outer belt during the September 2017 three-belt event have been presented in the form of flux versus L shell. As the change of local magnetic field in magnetosphere may result in significant flux increases and depletions, removing the adiabatic effects is necessary to figure out the exact acceleration, loss and radial transport process of the radiation belt population. Particle detector measurements provide us particle fluxes of different energy and pitch angles at different L shells ($j(E_k, \alpha, L)$). Converting them to phase space density (PSD) in the coordinate of three adiabatic invariants ($f(\mu, K, L^*)$) enables space physicists to differentiate various physical processes that drive the acceleration or loss of the radiation belt. Here μ is the first adiabatic invariant ($\mu = \frac{p_\perp^2}{2m_0B}$) describing the gyro motion of the particle and the second adiabatic invariant K, given by $K = I\sqrt{B_m}$, describes their bounce motion [see *Reeves et al.*, 2013; *Morley et al.*, 2013]. The quantity L^* is Roederer's generalized L shell [*Roederer*, 1970], which defines the geocentric radial location of the drift motion of magnetospheric particles.

Figure 3 (c) and (d) show the evolution of PSD as a function of L^* at fixed first and second adiabatic invariant ($\mu = 60$ MeV/G, $K = 0.3R_EG^{1/2}$), which correspond to the developing and fading-out stage of the three-belt structure respectively. Panel (e) and (f) are similar plots for $\mu = 120$ MeV/G and the same K value. Tsyganenko (TS) 04 geomagnetic field model [*Tsyganenko and Sitnov*, 2005] is adapted for the computation of K and L^* while in situ magnetic field strength from EMFISIS is used to calculate μ for each MagEIS energy and pitch angle channel. Fluxes of 600 keV electrons as a function of L shell during the same intervals have been plotted in panel (a) and (b). $\mu = 60$ MeV/G and 120 MeV/G are selected as they corresponding to ∼600 keV at $L^* = 3.5$ and 4.5 respectively, at which the fluxes of 600 keV remnant belt and external outer belt peaks (see Figure S2 for the $E_k(L^*)$ profile for the given μ and K).

As presented in Figure 3(e), after the depletion triggered by the solar wind pressure pulse at 2005UT on September 12, the outer belt at $L^* > 4$ replenished to its previous level, while phase space density at $L^* < 4$ remained to be low, thus forming a two-step-like radial PSD profile on September 14 (marked with number 1,2 and 3). Such an outer belt replenishment with limited radial penetration resulted in the additional peak of flux radial profile at $L \sim 4.5$ in 600 keV channel, and therefore the three-belt structure. The filling-up of the external outer belt continued in the following two days (marked with number 4 and 5) and the phase space density of 120 MeV/G electrons in the external outer belt exceeded its pre-event value on September 16.

For the remnant belt population, phase space density profiles presented in Figure 3(c) and (d) indicate that they were suffering from continuous loss process throughout the whole three-belt event. As marked with number 6,7,8 and 9, the phase space density of 60MeV/G electrons at $L^* = 3.5$ decreased gradually from $2 \times 10^{-4} MeV^{-3} cm^{-3}$ to $4 \times 10^{-5} MeV^{-3} cm^{-3}$ in 96 hours. The fast decay of the remnant belt and the replenishment of the external belt "destroyed" the three-belt structure. As shown in panel (b), (d) and (f), the two-step-like PSD profile disappeared as the damping of the remnant belt and the outer belt returned to be single-peaked, while the peak was composed of the new external outer belt. Note that during the whole time interval of interest, the radial gradient in phase space density profile of 60MeV/G electrons are mostly positive around the spatial extent of the remnant belt (in other words, $\frac{\partial f}{\partial L^*} |^{\mu=60MeV/G}_{K=0.3R_E G^{1/2}} > 0$ at $2.5 < L^* < 4$), which seems not in favor of net outward transport driven by radial diffusion. Thus such a continuous loss of remnant belt electrons are not likely to be simply explained with radial diffusion. Local loss mechanism (e.g. precipitation to atmosphere driven by wave-particle interactions by hiss waves or EMIC waves) is required for the fast decay of the remnant belt, which will be discussed in the following section.

5. Fast Decay of the Remnant Belt

Another note-worthy character of the sub-MeV three-belt structure is its relatively short time scale. Unlike the ultra-relativistic three-belt structures reported during the Van Allen Probe mission [e.g., *Baker et al.*, 2013b; *Mann et al.*, 2016; *Pinto et al.*, 2018], which could last for weeks, the three-belt structure of 600 keV electrons studied in this paper only lasted for 2-3 days. As discussed in the previous sections, the unenduring nature of the 600 keV three-belt structure in this case can be largely attributed to the fast decay of the remnant belt. In this section, the lifetime of the sub-MeV remnant belt is quantified and the possible mechanism that drives the decaying process is discussed.

The spin-averaged flux versus time profile of ∼600 keV electrons at the heart of the remnant belt (L=3.5, as marked with dashed black line in Figure 2(f)) has been plotted in Figure 4(a) in logarithmic scale. After the strong enhancement event during the intense storm on September 7 ∼ 9, the flux of ∼600 keV electrons at L=3.5 decayed monotonically in the following two weeks, which is consistent with the absence of the deep inward penetration of 60MeV/G electrons that reaches $L^* = 3.5$ (check Figure 3(c) and (d)). During the time interval of 600 keV three-belt structure, the flux profile fits well into an exponential decay. The mean lifetime τ evaluated from the function $j(t) = j_0 e^{-t/\tau}$ is 2.05 days. Note that such estimated lifetime is quite close to the theoretical prediction of hiss wave scattering by *Shprits et al.* [2013] (check Figure 2c in their paper) and empirical estimation by *Claudepierre et al.* [2020]. The ∼ 2 days lifetime of the remnant belt explains why the three belt structure no longer existed after September 15 0000UT. In other words, the flux of ∼600 keV electrons damps so fast at the heart of the remnant belt that the remnant belt became no longer comparable with the new external belt after days. Comparing with the lifetime of ultra-relativistic electron remnant belts estimated by *Pinto et al.* [2018], which is in an order of tens of days, the 600 keV remnant belt reported in this case presents a rather unstable trapping feature.

The energy dependence of wave-particle interaction is likely to explain the significant difference in lifetime of 600 keV and ultra-relativistic electron remnant belt. *Shprits et al.* [2013] suggested that ultra-relativistic electrons inside the remnant belt can remain unaffected by plasma waves for weeks, which is consistent with the statistics from Van Allen Probe measurements [*Pinto et al.*, 2018; *Claudepierre et al.*, 2020]. The energy-dependence of the electrons' lifetime at L=3.5 is presented in Figure 4(b). Lifetime increases as a function of energy throughout the energy range from 500 keV to >2 MeV. For sub-MeV electrons, the lifetime at L=3.5 lies below 5 days in this event. For electrons of energy greater than 1MeV, their lifetime measured in this case increases to the value in agreement with previous statistical results [cf. *Pinto et al.*, 2018, Figure 4 (left bottom)].

In order to further investigate the energy dependent physical processes of the remnant belt, the spectral evolution at the heart of the remnant belt during the sub-MeV three belt event is presented in Figure 4(c). The spectra of electrons with 90° local pitch angle measured by MagEIS and REPT at L=3.5 are combined and plotted in the same format as [cf. *Zhao et al.*, 2019a, Figure 2]. Bump-on-tail (BOT) distribution with flux minimum at ∼600 keV emerged gradually during the fading-out stage of the remnant belt. BOT distributions have been proven to be a consequence of particles' loss to atmosphere driven by hiss wave scattering [*Zhao et al.*, 2019a, b; *Ni et al.*, 2019]. *Zhao et al.* [2019a] and *Ni et al.* [2019] suggested that interaction with hiss waves inside the plasmapause could effectively scatter electrons with the energy of hundreds keV to the loss cone, which results in the BOT distributions. Statistical results by *Zhao et al.* [2019a] indicated that the BOT spectra are confined inside the plasmapause and take $\sim 1-2$ days to form. The emerging BOT distribution during the fading of the remnant belt in this event is consistent with those previous observations. The plasmapause derived from the spacecraft potential (plotted with the white line in Figure 2(f)) were mostly located at higher L shell than the remnant belt during the time interval. Hiss wave activities in the plasmasphere were also observed by Arase spacecraft (see Figure S3). Therefore we suggest that the hiss wave scattering could be an interpretation to the quick fading-out of the ∼600 keV remnant belt reported in this case. *Ripoll et al.* [2016]; *Zhao et al.* [2019a] also concluded that the forming of "S-shaped" inner boundary of the outer belt in energy-L shell spectrogram is a consequence of the energy-dependent hiss scattering. In the three-belt event we report, the "S-shaped" inner boundary of the remnant belt during its fading-out stage is also likely to be driven by the same physical process. At higher L shell, due to the leak of plasmaspheric hiss waves, the spectral evolution was dominated by the replenishing process and BOT distributions were not recorded at the heart of the external outer belt (see Figure 4(e)). The evolution of the electron energy spectra during 14-16 September was dominated by flux enhancement that reached >500 keV range.

6. Discussion

6.1. The Formation and Decay of Sub-MeV Three-belt Structure

In the previous sections we have presented detailed observational results of the sub-MeV three-belt event in September 2017. For ∼600 keV energy channel, which show clear three-belt structure, the evolutions at $L > 4$ (namely, the external outer belt) and $L < 4$ (remnant belt) are governed by different physical processes.

For the electrons at $L > 4$, fast depletion following the pressure pulse and subsequent replenishment built up the new external outer belt. The fast depletion after the strong pressure pulse (solar wind dynamic pressure upto 15nPa, Δ SYM/H upto +29nT) is likely to be driven by the magnetopause shadowing effect accompanied with the outward radial diffusion [e.g., *Turner et al.*, 2012, 2014; *Xiang et al.*, 2017]. High solar wind pressure is able to compress the magnetopause and the drift shell of particles at large L shell will encounter the magnetopause, leading to substantial loss at large L shell. After the passage of high pressure solar wind, radial diffusion driven by ULF waves could further deplete the phase space density of electrons at lower L shell although their drift orbit are not large enough to encounter the magnetopause.

As to the replenishing process of electrons in the external outer belt, its limited radial penetration depth is key to form the sub-MeV three-belt structure. In term of electron spectra (see Figure 4(c-e)), the flux enhancement of 500$\sim$800 keV electrons observed at the heart of the external outer belt did not penetrate to the remnant belt, which is consistent with the "V-shaped distributions with a remnant belt" type of $j(E_k, L)$ discussed in Section 3. In terms of PSD, the filling-up of 120MeV/G electron did not cover the whole outer belt zone, forming a two-step-like $f(L^*)\mid_{\mu,K}$ profile. Similar two-step-like PSD profile has also been recorded previously by THEMIS [*Turner et al.*, 2013] and Van Allen Probes observations (cf. Supplementary Figure 3 of *Mann et al.* [2016] and Figure 11 of *Da Silva et al.* [2019]), but for $\sim$1000s MeV/G electrons, which correspond to ultra-relativistic electrons at the heart of outer belt. In both cases the formation of such two-step-like PSD profile coexists with the development of ultra-relativistic three-belt structure (namely, 3.4 MeV channel on 6 September 2012 and 2.1 MeV channel on

25 September 2014). As addressed by *Mann et al.* [2016], the formation of a three-belt is sensitive to the penetration of ULF power, otherwise the merging of remnant belt and the external belt will result in a two-belt structure. The $L^* > 4$ part of the 60 MeV/G and 120 MeV/G electron PSD profile in this event did not show clear local peak during the refilling process, indicating that the formation of external outer belt within the Van Allen Probe orbital reach is possibly driven by pure radial transport [*Reeves et al.*, 2013]. However, since the evolution of PSD profile could be dominated by multiple processes and inevitable error in PSD calculation, the contribution of local acceleration could not be simply ruled out. Although diagnosing the exact acceleration mechanism of the external outer belt in this event is beyond the scope of this study, we would like to note that, similar to the electrons with first adiabatic invariant of thousands of MeV/G (ultra-relativistic), the two-step-like radial PSD profile of hundreds MeV/G electrons also denotes an L-dependent refilling process of sub-MeV electrons during the recovery of outer belt depletion.

For the sub-MeV electrons in the remnant belt, evolutions in PSD profile and energy spectrum indicate a gradual local loss process. Estimated lifetime of the 600 keV electrons at the heart of the remnant belt is around 2 days. The emerging BOT distribution with a local valley at $\sim$600 keV is consistent with the scenario that electrons were scattered to loss cone by hiss waves and precipitated to atmosphere during the vanishing of the remnant belt. The relatively short lifetime of the sub-MeV remnant belt comparing with the previous studied ultra-relativistic storage ring explains the unenduring nature of the sub-MeV three-belt structure, and somehow, the reason why it has not been easily noticed before this study.

Our scenario interpreting the mechanism of development and fading-out of the sub-MeV three-belt structure is summarized schematically in Figure 5(d). Sudden depletion of outer belt at large L shell leaves a remnant belt restricted within small L shell. The subsequent inward transport and/or the local acceleration at large replenished the large L shell region with a moderate penetration depth, resulting in a “second slot” between the external outer belt and the remnant belt. Such a three-belt structure can last for several days until the remnant belt are fully depleted by the gradual loss to atmosphere driven by wave-particle interaction. When the remnant belt is no longer recognizable, the radiation belt turns back to a two-belt structure, while the outer belt has been replaced by the newly formed external outer belt. Such scenario is similar to the formation of ultra-relativistic three belts [*Baker et al.*, 2013b; *Mann et al.*, 2016]. However, ultra-relativistic electrons in the remnant belt are mostly unaffected by the hiss wave and therefore fierce geomagnetic activties are needed to break down the pre-existing three-belt structure, while sub-MeV three-belt structure could fade out automatically in short time period due to the unenduring remnant belt under the efficient scattering by plasmaspheric hiss waves.

6.2. Electron Distributions During A Three-belt Event

Multiple pieces of peculiar features in the spatial and energy distributions of electrons appeared during the developing and fading-out stage three-belt event (double-peaked outer belt, two-step-like PSD profile, V-shaped $j(E_k, L)$ distribution with a remnant belt, BOT spectrum, etc.). It is easy for one to find that these various phenomena are strongly correlated. Here we recall the MagEIS measurement from an outbound pass of Van Allen Probe B during the time interval of sub-MeV three-belt structure. In Figure 5(b) the electron differential flux as a function of L shell and energy has been plotted, using the same data as Figure 2(d). The PSD as a function of L^* for $\mu = 60$ MeV/G and $K = 0.3 R_E G^{1/2}$ electrons is plotted at left and the fluxes as a function of L for 349.8 keV, 599.6 keV and 1049.8 keV energy channel are plotted at right. As discussed by *Reeves et al.* [2016]; *Turner et al.* [2019], the penetration depth in L shell of outer belt enhancement in response to storms is energy dependent. Lower energy channels always have a deeper penetration depth and a stronger enhancement, leading to a positive slope in the inner boundary of the outer belt, which composes the right part of the V-shaped boundary in $j(E_k, L)$ spectrogram. In the sub-MeV three-belt event we studied, such kind of V-shaped boundary also exists between the inner belt and the external outer belt. One thing additional to the V-shaped structure is the remnant belt. Unlike the total extinction of outer belt populations on September 7, 2017, the dropout event on September 12 is not significant at $L \leq 4$. Therefore a remnant belt structure which peaks at $L \sim 3.5$ was superposed above the V-shaped distribution, forming a peculiar "V-shaped distribution with a remnant belt" spectrogram. Between the inner belt and growing external outer belt, the inner boundary of the fading-out remnant belt show a S-shaped structure. Such an S-shaped structure indicates that the remnant belt was depleted by an energy-dependent process [*Ripoll et al.*, 2016]. High energy electrons are able to stay for a long time (as previously discussed in Section 5) and form a local flux maximum in energy spectrum. Therefore the BOT distribution was observed inside the remnant belt. The gradual shift of flux minimum energy to higher energy channels of BOT spectra presented in Figure 4(c) could also be explained by the competing between emerging external outer belt with a V-shaped inner boundary (which lifts the low energy end of the spectrum) and the continuous hiss scattering (which depletes the flux at moderate energy channels).

Since the slice of $j(E_k, L)$ at fixed E_k gives the radial profile of electron flux, such a "V-shaped with a remnant belt" spectrogram could help us in understanding the energy-dependent morphology of the outer belt (see Figure 5(c) and please check Figure S1 for the time evolutions of radiation belt at different energy channels). On one hand, the external belt produced by the replenishing process did not reach energy channels above 600 keV at that time, while the remnant belt still survived, which explains the single outer belt with a peak at $L \sim 3.5$ in 1049.8 keV channel (also in 891.9 keV and 1541.0 keV channel). On the other hand, the replenishing process was sufficient at 349.8 keV and 466.8keV channel. At the same time, hiss wave scattering were efficiently removing electrons inside the plasmasphere (forming an S-shaped boundary in panel (b) and Figure 2(d)). Therefore the flux radial profile of 349.8 keV and 466.8keV channel at the time point was also single-peaked, but the peak was located at $L \sim 4.5$. In brief, the radial profile of >1 MeV channel represents the "old" outer belt surviving from the dropout at SSC and the profile of <500 keV channel represents the "new" belt produced by the recovery phase of the moderate storm. For the transitional energy channel, 500 keV$\sim$800 keV in this case, the components of the new belt and the old belt are comparable, but peaking at different L shell, which results in a double-peaked radial profile of outer belt. We note that such flux profile looks quite similar to a superposition of the normalized profile in <500 keV and >1 MeV channels. For the electrons in the transitional energy channels, both the replenishing of external outer belt and the decaying at $3 < L < 4$ are moderate, which is able to form an external belt at high L shell and meanwhile leaves the remnant belt population distinctive.

The two-step-like PSD profile, which has been observed previously but not being widely discussed, could also be illustrated from the prospective of $j(E_k, \alpha, L) \rightarrow f(\mu, k, L^*)$. As the white dashed-and-dotted curve in Figure 5(b) marked, the constant μ line of certain first adiabatic invariant could confront both the inner edge of the remnant belt and the external outer belt. Then there is no surprise that there are two steep positive radial gradient in $f(\mu, k, L^*) \mid_{\mu,k}$ and therefore a two-step-like PSD radial profile. Note that the color-coded fluxes that white dashed-and-dotted curve crosses in this panel do not accurately correspond to the flux that is converted to $f(\mu, k, L^*) \mid_{\mu,k}$, as the pitch angle is varying along the L shell for a given k value. However it will not bring much difference to our illustration as the inner boundaries of both belts are distinctive in $j(E_k, L)$ space at all pitch angle in this case.

7. Conclusions

To conclude, in this study we report the existence of three-belt structure in sub-MeV energy channel. Double-peaked outer belt in 500 keV∼800 keV energy range were documented by Van Allen Probes after a moderate storm that followed the September 2017 intense storm and lasted for $2 \sim 3$ days. The main results we get from this case study are the following:

1. Three-belt structure is not restricted to ultra-relativistic electrons and could be highly energy dependent. The formation of the sub-MeV three-belt structure is a combination of a partial outer belt dropout and a replenishing process that do not penetrate deep into the remnant belt, which does not differ much from the ultra-relativistic three-belt cases. More attention on sub-MeV energy range from the radiation belt community will lead to a more complete and comprehensive knowledge of radiation belt dynamics.

2. The energy dependence of three-belt structure occurrence can be explained by energy and L shell dependence in the replenishing and loss processes. A transition energy channel at which the emerging "new" outer belt component and "old" component survived from flux dropout are comparable in intensity and distinctive in L shell will show a three-belt structure.

3. The remnant of sub-MeV electrons seems not as persistent as the ultra-relativistic remnant belts reported in previous studies. The fast decaying of the remnant belt is likely to be a result of particles' loss to atmosphere driven by hiss wave scattering, which is evidenced by bump-on-tail spectra. The short-lived nature of sub-MeV remnant belt may explain why sub-MeV three-belt structures are hard to get recognized from electron flux profile plotted for a large time scale.

4. Novel types of radiation belt electron distributions arise during the sub-MeV three-belt phase. A remnant belt population in addition to the typical V-shaped distribution in $j(E_k, L)$ is a typical spectrogram for sub-MeV three-belt event. The inner boundary of the remnant belt can further evolve to S-shape during the fading-out stage of the three-belt structure. These novel spatial-energy distributions give rise to a two-step-like PSD radial profile at certain first adiabatic invariant that meets the inner edges of both the remnant belt and the external outer belt.

8. Acknowledgement

This work was supported by National Natural Science Foundation of China (41421003, 41627805). R. Rankin acknowledges financial support from the Canadian Space Agency and NSERC. Processing and analysis of the MagEIS and REPT data was supported by Energetic Particle, Composition, and Thermal Plasma (RBSP-ECT) investigation funded under NASA's Prime contract no. NAS5-01072. All RBSP-ECT data are publicly available at the Web site http://www.RBSP-ect.lanl.gov/. RBSP-EFW and RBSP-EMISIS data used to derive plasmapause location and phase space denisty are also publicly available at the Web sites http://www.space.umn.edu/rbspefw-data/ and http://emfisis.physics.uiowa.edu/data/index/. BD-IES data are publicly available at the Web site http://www.beidou.gov.cn/yw/gfgg/201912/.

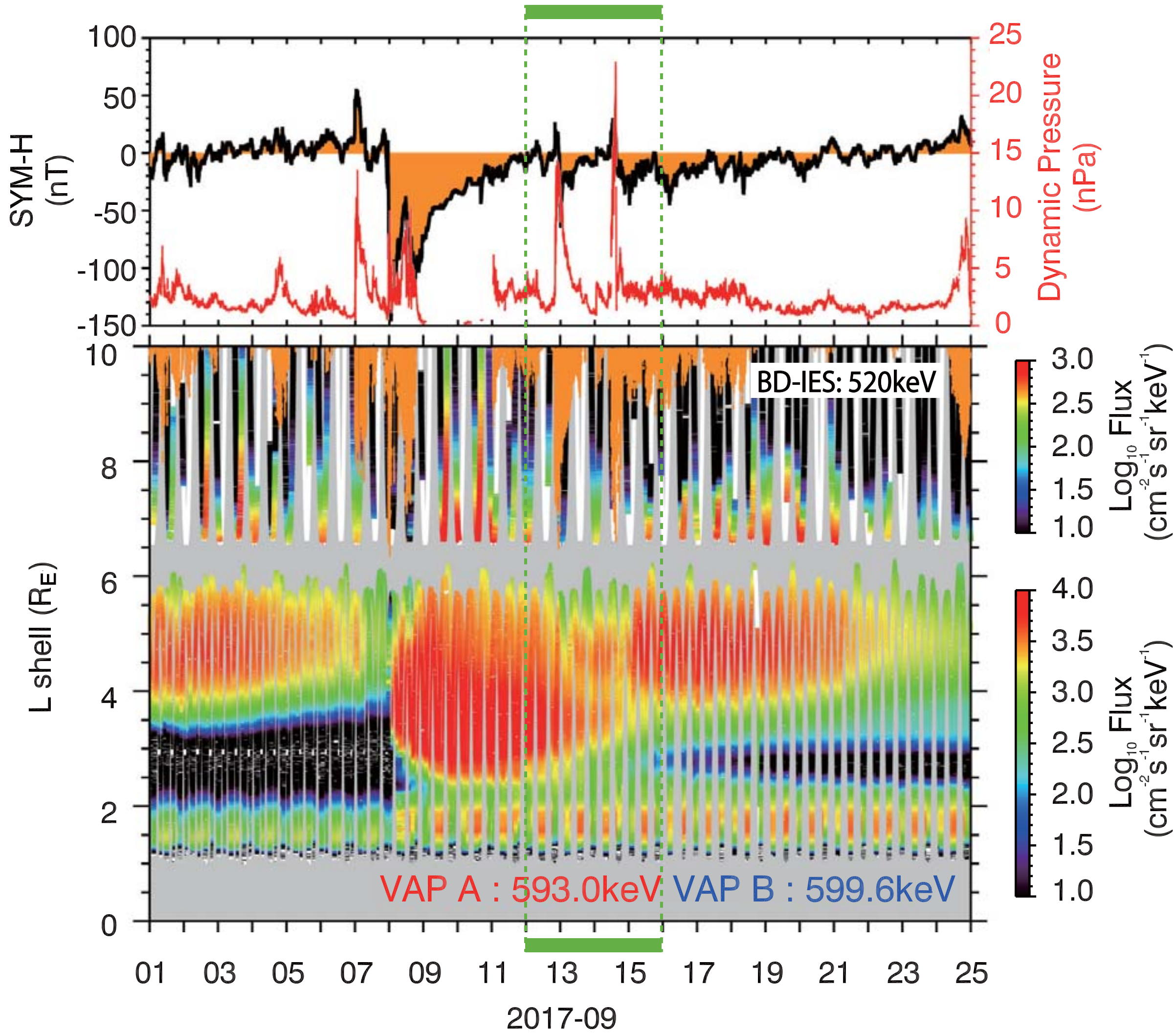

Figure 1. (Top) Geomagnetic *SYM-H* index (in black) and the solar wind dynamic pressure from OMNI data (in red) during 1 - 24 September 2017. (Bottom) Spin-averaged fluxes of ∼600 keV electrons using data from MagEIS instrument on Van Allen Probes and omni-directional electron fluxes of 520 keV electrons from IES instrument on Chinese IGSO satellite. Time intervals lack of data coverage are plotted with white lines. Areas shaded by orange color in the bottom panel show the magnetopause location calculated with OMNI data based on the empirical model from *Shue et al.* [1998].

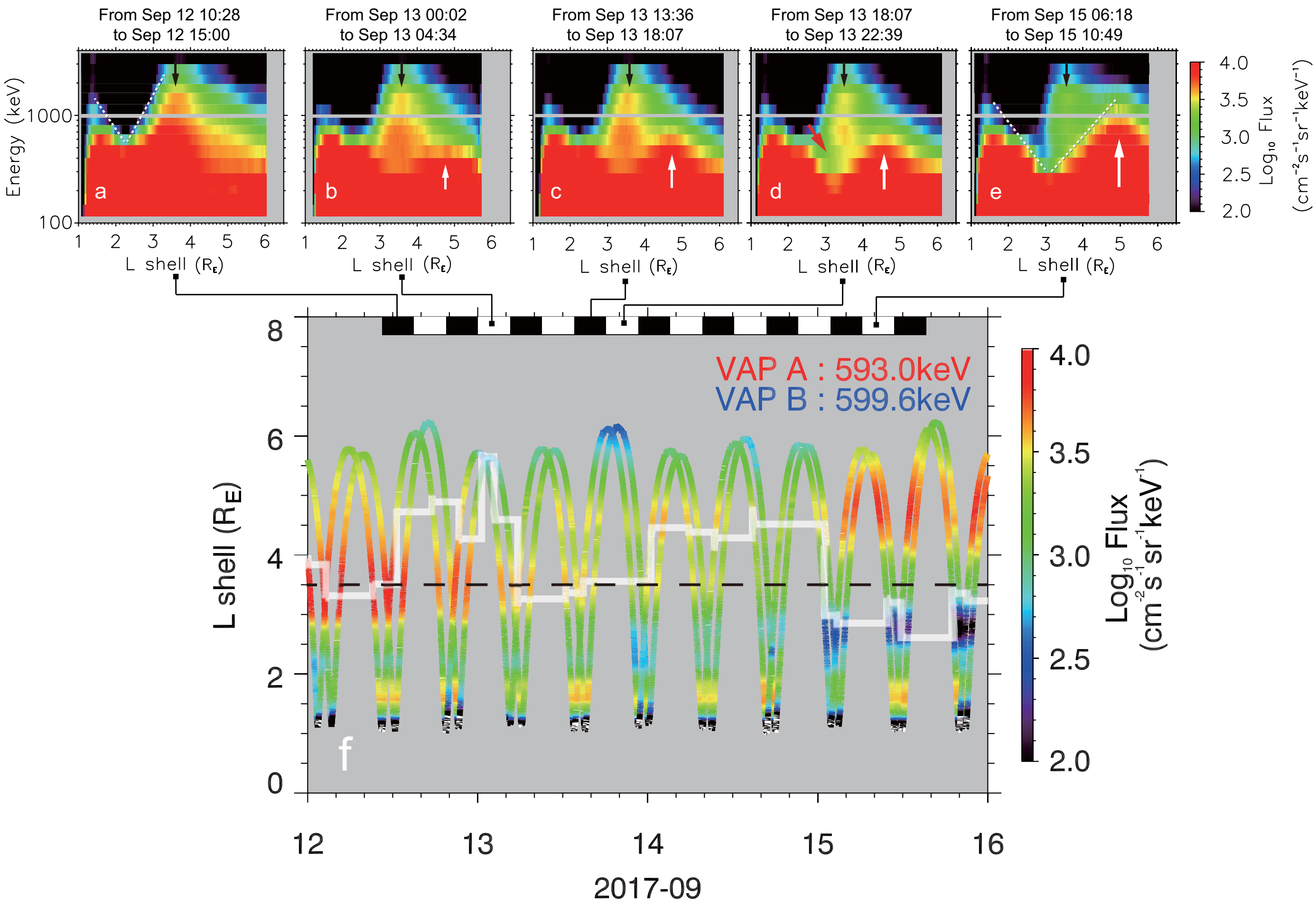

Figure 2. A zoom-in view of the MagEIS flux data during the 600 keV three-belt phase in September 2017 (time interval marked with green dashed lines in Figure 1). (a-e) Radiation belt flux as a function of L shell and energy for selected Van Allen Probe B passes. Black arrows indicate the position of remnant belt ($L = 3.5$) and white arrows indicate the growing external outer belt populations. (f) Zoom-in plot of the $\sim$ 600keV electron fluxes as a function of time and L shell from Van Allen twin Probes. White line shows the plasmapause location derived from the spacecraft potential data from EFW-B. Black dashed line at $L = 3.5$ indicates the remnant belt maximum.

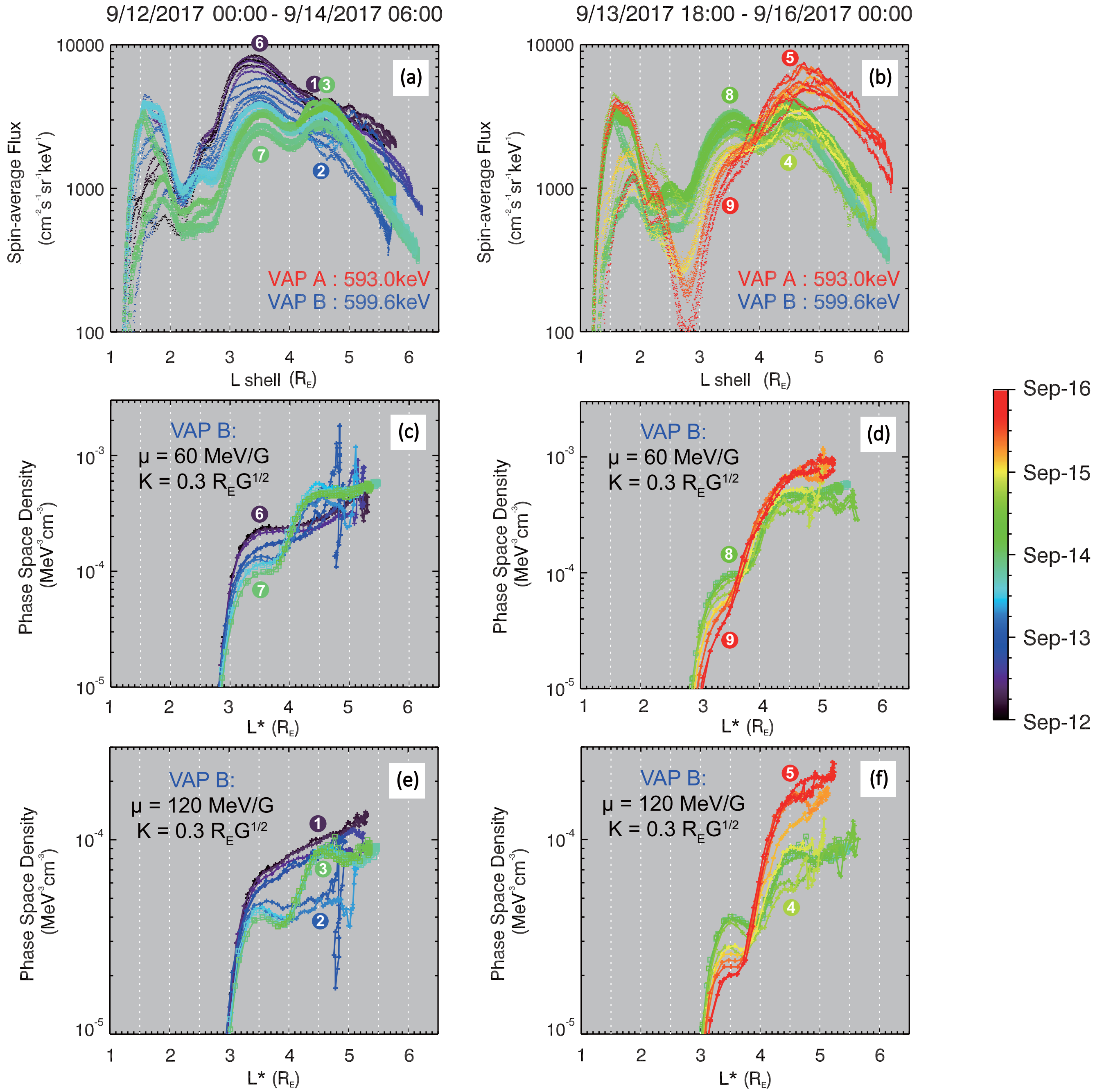

Figure 3. Differential flux and phase space density evolution during the developing (left column) and fading out (right column) stage of the 600 keV 3-belt structure. (a) Flux of ∼600 keV electrons measured by MagEIS-A and -B as a function of L shell during the developing stage of 3-belt structure. (c) Temporal sequence of electron phase space density as a function of L* at given $\mu = 60MeV/G$ and $K = 0.3R_EG^{1/2}$ during the developing stage of 3-belt structure. 60 MeV/G corresponds to ∼600 keV at L* = 3.5. (e) Similar to (c) but for $\mu = 120MeV/G$, which corresponds to ∼600 keV at L* = 4.5. (b, d and f) Same format as left panels, depicting the fading out stage of the 3-belt structure.

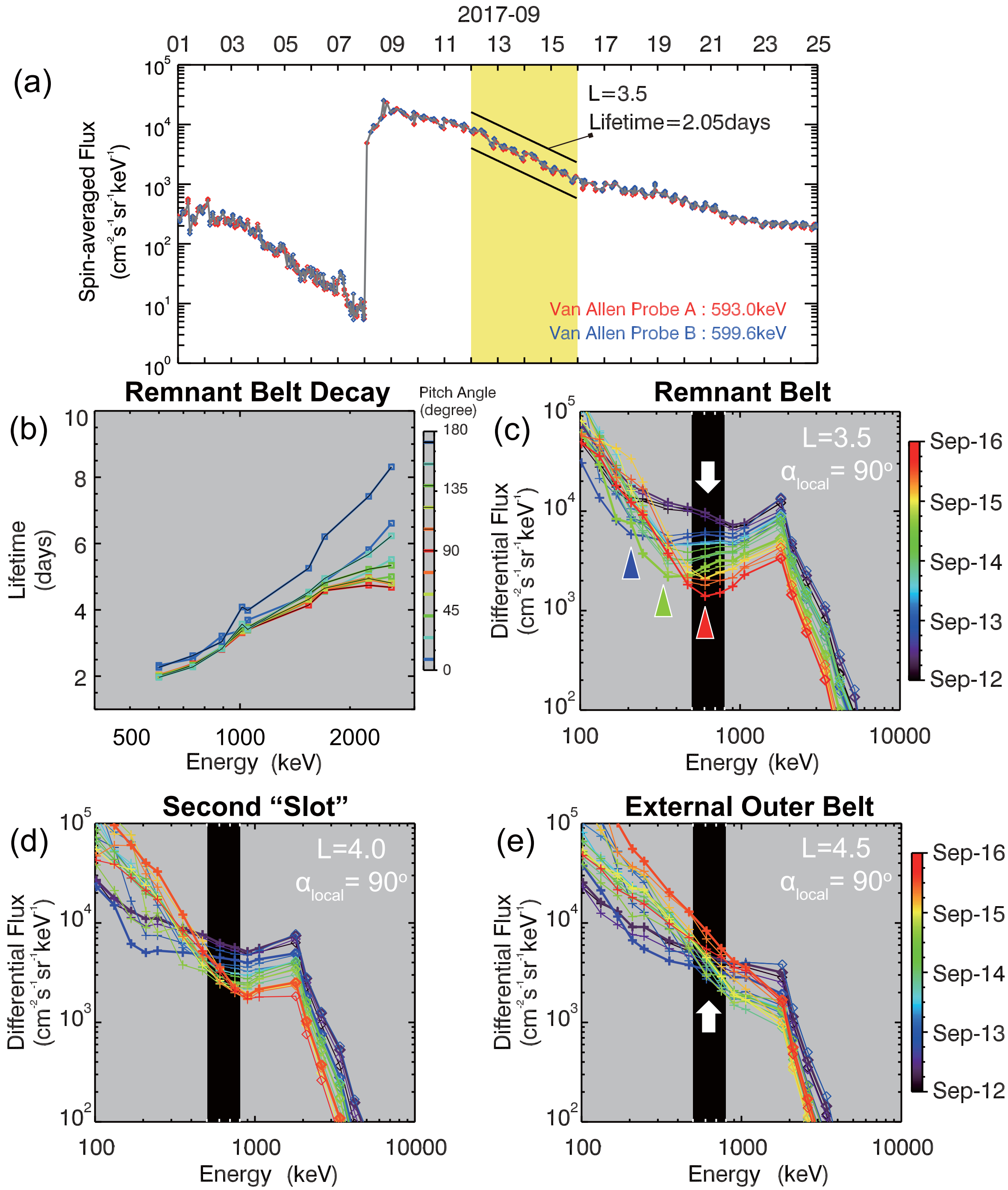

Figure 4. (a) Time series of spin-averaged flux of ~ 600 keV electrons at the heart of the remnant belt ($L = 3.5 \pm 0.01$) recorded by Van Allen Probes and its best fit of the decay rate during the time interval between 12 - 15 September (marked in yellow). (b) Lifetime as a function of energy and pitch angle at $L = 3.5 \pm 0.01$. (c-f) Energy spectra evolutions during the time interval of interest from MagEIS-B (crosses) and REPT-B (diamonds) at L=3.5, 4.0 and 4.5. Colored spikes indicate the energy of flux minimum. Black areas mark the energy range showing three-belt structure.

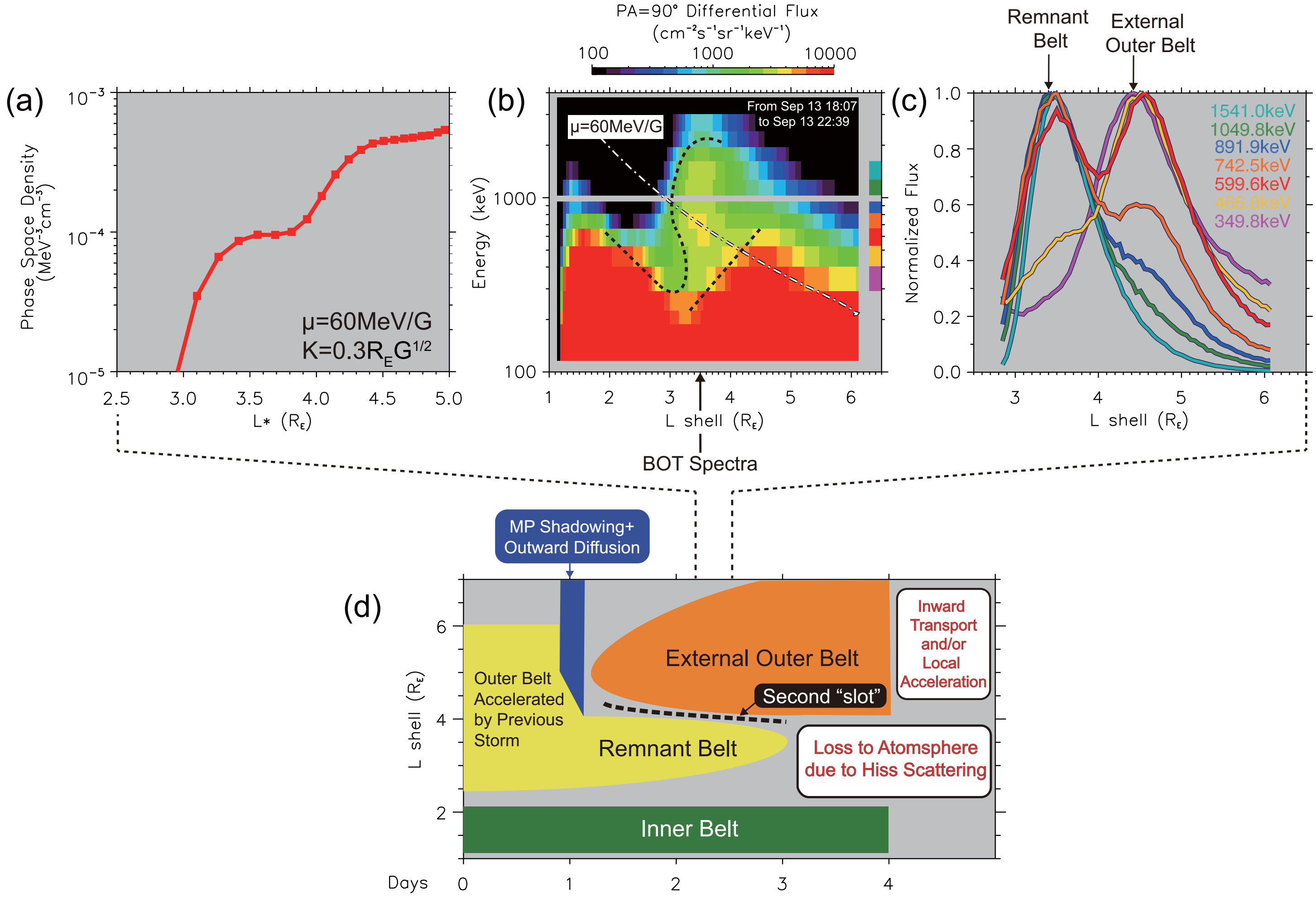

Figure 5. (a-c) Snapshots of the radiation belt during the 3-belt phase: (b) gives the flux of 90° pitch angle electrons as a function of energy and L shell (same data as Figure 2d). Black dashed curves mark the energy dependence of "S-shaped" inner boundary of the remnant belt and "V-shaped" inner boundary of the external outer belt. White dashed-and-dotted curve gives the energy as a function of L shell for a set of constant μ and K. Panel (c) gives the radial profile of normalized flux in the outer belts for selected energy channels in panel (b). Panel (a) gives the PSD profile against L* for $\mu = 60MeV/G$ and $K = 0.3R_EG^{1/2}$, which corresponds to the white dashed lines in panel (b). (d) A schematic diagram showing the processes forming and fading the three-belt structure below 1 MeV.

References

Baker, D., et al., The relativistic electron-proton telescope (rept) instrument on board the radiation belt storm probes (rbsp) spacecraft: Characterization of earth's radiation belt high-energy particle populations, *Space Science Reviews*, *179*(1-4), 337–381, doi:10.1007/s11214-012-9950-9, 2013a.

Baker, D., et al., A long-lived relativistic electron storage ring embedded in earth's outer van allen belt, *Science*, *340*(6129), 186–190, 2013b.

Blake, J., et al., The magnetic electron ion spectrometer (mageis) instruments aboard the radiation belt storm probes (rbsp) spacecraft, *Space Science Reviews*, pp. 1–39, 2013.

Claudepierre, S., et al., A background correction algorithm for van allen probes mageis electron flux measurements, *Journal of Geophysical Research: Space Physics*, *120*(7), 5703–5727, 2015.

Claudepierre, S. G., Q. Ma, J. Bortnik, T. P. O'Brien, J. F. Fennell, and J. B. Blake, Empirically estimated electron lifetimes in the earth's radiation belts: Comparison with theory, *Geophysical Research Letters*, *47*(3), e2019GL086,056, 2020.

Da Silva, L. A., et al., Contribution of ulf wave activity to the global recovery of the outer radiation belt during the passage of a high-speed solar wind stream observed in september 2014, *Journal of Geophysical Research: Space Physics*, *124*(3), 1660–1678, 2019.

Farrugia, C., V. Jordanova, M. Thomsen, G. Lu, S. Cowley, and K. Ogilvie, A two-ejecta event associated with a two-step geomagnetic storm, *Journal of Geophysical Research: Space Physics*, *111*(A11), 2006.

Kletzing, C., et al., The electric and magnetic field instrument suite and integrated science (emfisis) on rbsp, *Space Science Reviews*, pp. 1–55, 2012.

Mann, I. R., et al., Discovery of the action of a geophysical synchrotron in the earth's van allen radiation belts, *Nature communications*, *4*, 2013.

Mann, I. R., et al., Explaining the dynamics of the ultra-relativistic third van allen radiation belt, *Nature Physics*, *12*(10), 978, 2016.

Mauk, B., N. J. Fox, S. Kanekal, R. Kessel, D. Sibeck, and A. Ukhorskiy, Science objectives and rationale for the radiation belt storm probes mission, in *The Van Allen Probes Mission*, pp. 3–27, Springer, 2014.

Morley, S., M. Henderson, G. Reeves, R. Friedel, and D. Baker, Phase space density matching of relativistic electrons using the van allen probes: Rept results, *Geophysical Research Letters*, *40*(18), 4798–4802, 2013.

Ni, B., et al., Parametric sensitivity of the formation of reversed electron energy spectrum caused by plasmaspheric hiss, *Geophysical Research Letters*, *46*(8), 4134–4143, 2019.

Pinto, V. A., J. Bortnik, P. S. Moya, L. R. Lyons, D. G. Sibeck, S. G. Kanekal, H. E. Spence, and D. N. Baker, Characteristics, occurrence, and decay rates of remnant belts associated with three-belt events in the earth's radiation belts, *Geophysical Research Letters*, *45*(22), 12–099, 2018.

Reeves, G., et al., Electron acceleration in the heart of the van allen radiation belts, *Science*, *341*(6149), 991–994, 2013.

Reeves, G. D., et al., Energy-dependent dynamics of kev to mev electrons in the inner zone, outer zone, and slot regions, *Journal of Geophysical Research: Space Physics*, *121*(1), 397–412, 2016.

Ripoll, J.-F., et al., Reproducing the observed energy-dependent structure of earth's electron radiation belts during storm recovery with an event-specific diffusion model, *Geophysical Research Letters*, *43*(11), 5616–5625, 2016.

Roederer, J. G., *Dynamics of geomagnetically Trapped radiation*, Springer-Verlag, New York, 1970.

Shprits, Y. Y., D. Subbotin, A. Drozdov, M. E. Usanova, A. Kellerman, K. Orlova, D. N. Baker, D. L. Turner, and K.-C. Kim, Unusual stable trapping of the ultrarelativistic electrons in the van allen radiation belts, *Nature Physics*, *9*(11), 699, 2013.

Shue, J.-H., et al., Magnetopause location under extreme solar wind conditions, *Journal of Geophysical Research: Space Physics*, *103*(A8), 17,691–17,700, 1998.

Spence, H. E., et al., Science goals and overview of the radiation belt storm probes (rbsp) energetic particle, composition, and thermal plasma (ect) suite on nasa's van allen probes mission, *Space Science Reviews*, *179*(1-4), 311–336, 2013.

Tsyganenko, N., and M. Sitnov, Modeling the dynamics of the inner magnetosphere during strong geomagnetic storms, *Journal of Geophysical Research: Space Physics*, *110*(A3), 2005.

Turner, D., V. Angelopoulos, W. Li, M. Hartinger, M. Usanova, I. Mann, J. Bortnik, and Y. Shprits, On the storm-time evolution of relativistic electron phase space density in earth's outer radiation belt, *Journal of Geophysical Research: Space Physics*, *118*(5), 2196–2212, 2013.

Turner, D., et al., On the cause and extent of outer radiation belt losses during the 30 september 2012 dropout event, *Journal of Geophysical Research: Space Physics*, *119*(3), 1530–1540, 2014.

Turner, D., et al., The response of earth's electron radiation belts to geomagnetic storms: Statistics from the van allen probes era including effects from different storm drivers, *Journal of Geophysical Research: Space Physics*, 2019.

Turner, D. L., Y. Shprits, M. Hartinger, and V. Angelopoulos, Explaining sudden losses of outer radiation belt electrons during geomagnetic storms, *Nature Physics*, *8*(3), 208–212, 2012.

Van Allen, J. A., The geomagnetically trapped corpuscular radiation, *J. Geophys. Res.*, *64*, 1683–1689, 1959.

Van Allen, J. A., and L. A. Frank, Radiation around the Earth to a radial distance of 107,400 km, *Nature*, *183*, 430–434, 1959.

Van Allen, J. A., G. H. Ludwig, E. C. Ray, and C. E. McIlwain, Observations of high intensity radiation by satellites 1958 Alpha and Gamma, *Jet Propulsion*, *28*, 588–592, 1958.

Xiang, Z., W. Tu, X. Li, B. Ni, S. K. Morley, and D. Baker, Understanding the mechanisms of radiation belt dropouts observed by van allen probes, *Journal of Geophysical Research: Space Physics*, *122*(10), 9858–9879, 2017.

Yuan, C., and Q. Zong, The double-belt outer radiation belt during cme-and cir-driven geomagnetic storms, *Journal of Geophysical Research: Space Physics*, *118*(10), 6291–6301, 2013.

Zhao, H., et al., Characterization and evolution of radiation belt electron energy spectra based on the van allen probes measurements, *Journal of Geophysical Research: Space Physics*, 2019a.

Zhao, H., et al., Plasmaspheric hiss waves generate a reversed energy spectrum of radiation belt electrons, *Nature Physics*, *15*(4), 367, 2019b.

Zong, Q., Y. Wang, H. Zou, L. Wang, R. Rankin, and X. Zhang, New magnetospheric substorm injection monitor: Image electron spectrometer on board a chinese navigation igso satellite, *Space Weather*, *16*(2), 121–125, 2018.

Zong, Q., et al., Radial propagation of magnetospheric substorm-injected energetic electrons observed using a bd-ies instrument and van allen probes, *Science China Earth Sciences*, *59*(7), 1508–1516, 2016.

Zou, H., et al., Imaging energetic electron spectrometer onboard a chinese navigation satellite in the inclined geo orbit, *Science China Technological Sciences*, *61*(12), 1845–1865, 2018.